

Strain Localization Behavior of Cold-Rolled Deep-Drawing Steels

Mert Efe*

Department of Metallurgical and Materials Engineering, Middle East Technical University, 06800, Ankara, Turkey
*mefe@metu.edu.tr

Received: 16 October 2018

Accepted: 12 February 2019

DOI: 10.18466/cbayarfbe.471039

Abstract

With the purpose of defining optimal microstructure and texture for higher quality in deep-drawing operations of cold-rolled steels; this study monitors and analyses the micro- and macro-scale deformation behavior of DC04 grade cold-rolled steel sheets under uniaxial tension and biaxial stretching. An in-plane biaxial test setup capable of observing and measuring the deformation is utilized for obtaining strain maps at the micro- and macro-scale. Strain maps at the micro-scale are then compared with texture and microstructure data obtained before and after the deformation. Results show strain localization to the interior of grains under both strain paths, as opposed to the common grain boundary localization observed in the literature. Remnants of the α fiber components in the initial γ fiber texture, especially grains with $\{100\}\langle 110 \rangle$ orientations, are the likely sources of the localizations as they allow deformation in the sheet thickness direction. While these localizations do not appear to be critical for macro-scale formability, their suppression should be helpful in preventing surface defects and local fracture. Total elimination of α fiber components from the initial texture is proposed as a way preventing micro-scale localizations.

Keywords: Forming, DC04, anisotropy, DIC, texture.

1. Introduction

Deep-drawing steels are low carbon, interstitial-free steels known for their excellent formability. They have low strength but a good strain-hardening exponent and total ductility; making them suitable for the complex deep-drawn automotive parts such as fenders, side panels, floor panels, and door panels [1]. As they are mostly supplied in cold-rolled form, they have a characteristic γ fiber texture $\langle 111 \rangle // ND$ yielding in perpendicular anisotropy (i.e. high r values) [1, 2]. The combination of these properties make the forming operations of these steels straightforward and engineers often neglect the microstructural effects when designing their forming processes and establishing the forming limits of the material.

As with all the deformation processes, forming limits in deep-drawing are reached when a plastic instability develops in the part. This instability usually originates from the thickness variations in the sheet and presents itself as a local neck. The strain localizes within the neck and quickly reaches the fracture strain of the material, leading to the cracking and fracture in the neck region [3]. On the other hand, some materials are known to develop plastic instabilities due to their microstructure, texture and environmental conditions. As an example, texture softening due to the favorably oriented grains in the microstructure can lead to the plastic instabilities [4]. Texture instabilities by their nature start at the microstructural level. Materials with

complex microstructures or limited deformation mechanisms can have “hard” and “soft” phases or grains in their microstructures, which can lead to deformation incompatibilities [5]. These incompatibilities usually cause strain localizations at phase or grain boundaries [5, 6]. Independent of their source of origin, strain localizations may initiate local fractures and limit the global formability of the material [5, 7]. Moreover, the localizations can also result in ridging, roping and stretcher marks, worsening the desired surface finish of the sheet products [5, 8].

Recent studies on the microstructure related strain localization behavior focus mostly on alloys with multiple phases and materials with limited formability [5, 9, 10]. Aluminum alloys have also been of an interest [3]. There are limited studies available on materials with sharp texture and anisotropy. These materials may exhibit a different localization behavior, as it will be hard to find “hard” and “soft” grains within the microstructure. Moreover, there are no studies on the localization behavior of mild steels. While the macro-scale formability is well established in these steels, in this study possible effects of microstructure and texture on the local formability are investigated together with their possible relations to the global formability. Sheets of DC04 grade, deep-drawing steel are tested by an in-plane biaxial tension setup capable of stretching sheet metals along multiple strain paths. Strain distributions and localizations are quantified by plotting strain maps at millimeter and micrometer

scales. Strain maps at the micro-scale are also correlated with the electron backscatter diffraction (EBSD) orientation maps of the microstructure before and after the deformation in order to identify the possible sources of localizations.

2. Materials and Methods

2-mm-thick sheets of DC04 in cold-rolled form were supplied from Erdemir, Turkey. DC04 contains maximum 0.08 wt% C, 0.035 wt% P, 0.035 wt% S and 0.40 wt% Mn. For microstructure characterization, samples from the sheet were prepared by standard metallographic techniques and imaged by a FEI Quanta 200 FX scanning electron microscope equipped with EDAX EBSD camera and OIM software. The standard cleanup procedures in the OIM were followed. EBSD data of the as-received sample shows the grain size, grain orientation and (111) pole figure of the micro-texture (Figure 1). The initial grain size is $\sim 30 \mu\text{m}$. Due to the cold-rolling, the sheet has a characteristic γ fiber texture with $\{111\}\langle 112 \rangle$ and $\{111\}\langle 110 \rangle$ components [1, 11]. The α fiber texture components $\{100\}\langle 110 \rangle$ are scarce, indicating that the sheet was subjected to an annealing treatment to intensify the γ fiber components [1, 11]. As expected from an annealing treatment, the grain size is fine and homogenous and the grains are equiaxed.

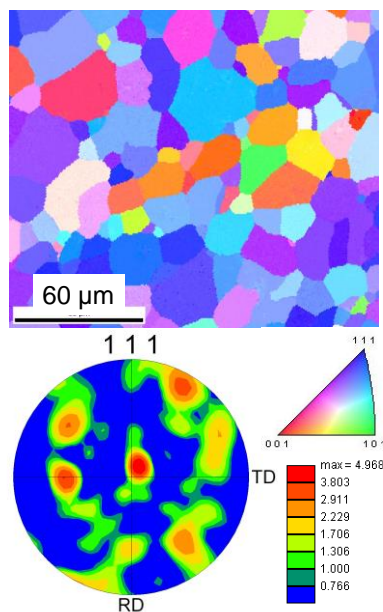


Figure 1. EBSD orientation map and (111) pole figure for the as-received sheet from the RD-TD plane.

As-received sheet was also tensile tested according to the ASTM E8 standard. Figure 2 shows the typical engineering stress-strain curve with average mechanical properties tabulated as an inset. The sample has exceptional ductility with a relatively high strain hardening exponent ($n = 0.21$).

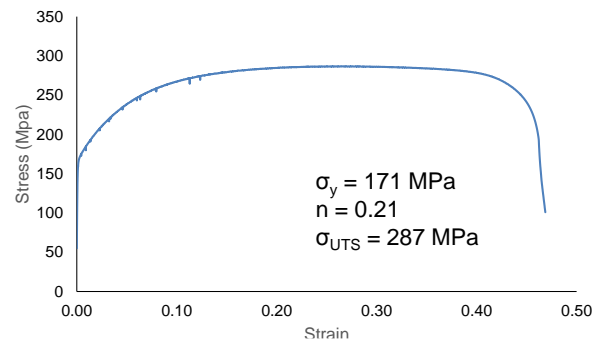


Figure 2. Representative engineering stress-strain curve of the as-received sheet.

After the characterization of the as-received sheet, cruciform samples were cut by laser-jet for formability testing. Samples as shown in Figure 3 have a reduced cross-section (pit) for collection of strains and stresses at the sample center. The pit was milled and has a diameter of 2 mm, allowing macro- and micro-scale testing. After milling, the sample surface was electropolished for 25 seconds with a Struers A2 Electrolyte (600 ml Ethanol, 150 ml 2-Butoxyethanol, 50 ml Perchloric acid (60%), 200 ml Water) in a Struers Lectropol-5 machine operating at 60 V. For macro-scale testing and imaging, the sample surfaces were sprayed by a paint solution containing 30% of acrylic paint and 70% of acetone, which resulted in randomly distributed $\sim 20 \mu\text{m}$ size black dots (speckles) when sprayed with an air brush at 10 cm distance from the sample surface. For micro-scale testing and imaging, sample surfaces were further electroetched for 12 s by using the same solution and machine, but this time with 5 V. The electro-etching both resulted in necessary features for strain characterization and allowed visualization of the grains and their boundaries.

Samples were then attached to the testing apparatus that was integrated to a Shimadzu Bending Test Machine with a capacity of 10 kN (Fig. 4). This apparatus converts the vertical compression force from the test machine to horizontal stretching. In this study, the samples were either pulled by uniaxial tension by attaching two of the sample arms to the apparatus, or by equibiaxial tension by attaching all arms of the sample to the apparatus. The arms of the apparatus had equal length and this ensured application of equal forces to each arm of the sample. Forces during the tests were also monitored by load cells attached to each arm of the apparatus.

Strain measurements and mapping were accomplished by an imaging unit attached to the apparatus (Fig. 4). Few hundred images were collected during the tests and later analyzed by a 2D digital image correlation (DIC) software named Ncorr. The entire pit base was imaged for macro-scale, whereas an area of $\sim 500 \times 500 \mu\text{m}^2$ was imaged for the micro-scale by zooming in to the pit base. The software tracks the speckle pattern on the sample surface between the consecutive images and

calculates the displacement and strains by using correlation algorithms. Details of the sample preparation, testing, and strain measurements can be found in a previous publication [12]. Overall, spatial resolution of the DIC is $96\ \mu\text{m}$ for the macro-scale and $10\ \mu\text{m}$ for the micro-scale based on the subset radius. However, actual resolutions are even finer for both scales as it was possible to fit few speckles or features inside the subsets.



Figure 3. Cruciform shaped test samples. The sample contains a pit at the center and the base of pit serves as the gauge area.

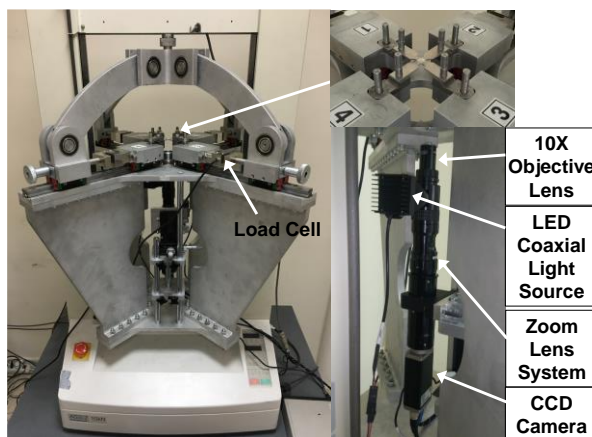


Figure 4. Test apparatus and the imaging unit used for testing and strain mapping.

3. Results and Discussion

Figure 5 compares the strain distribution at macro- and micro-scale in samples tested under uniaxial tension. In both samples, the average major strain is $\varepsilon_1 \sim 0.13$ and minor strain $\varepsilon_2 \sim -0.07$. Assuming $\varepsilon_1 \approx \bar{\varepsilon}$ under uniaxial tension, the equivalent strain is also 0.13. While the strain distribution is relatively uniform at the macro-scale (Fig. 5a), there are strain localized spots at the micro-scale (Fig. 5b). Difference between the maximum and minimum strains reaches to $\sim 3x$ (3 times) at this scale. Deviation from the average strain is $\sim 1.5x$ for both maximum and minimum strains. Despite the rather uniform microstructure and exceptional formability of the deep-drawing steel, it is still possible to observe considerable localizations, indicating that the local

microstructure and texture have an important role in controlling the deformation at the micro-scale.

At the micro-scale, deformation seems to localize inside of the grains rather than the grain boundaries. In literature, the common strain localization locations have been documented as the grain boundaries [5, 6]. The behavior in the cold-rolled steel is somewhat different from the common observations. Highly textured microstructures can be the reason of this behavior. Most of the grains have similar orientations and this may reduce the strain incompatibilities between the grains, eliminating localizations to the grain boundaries.

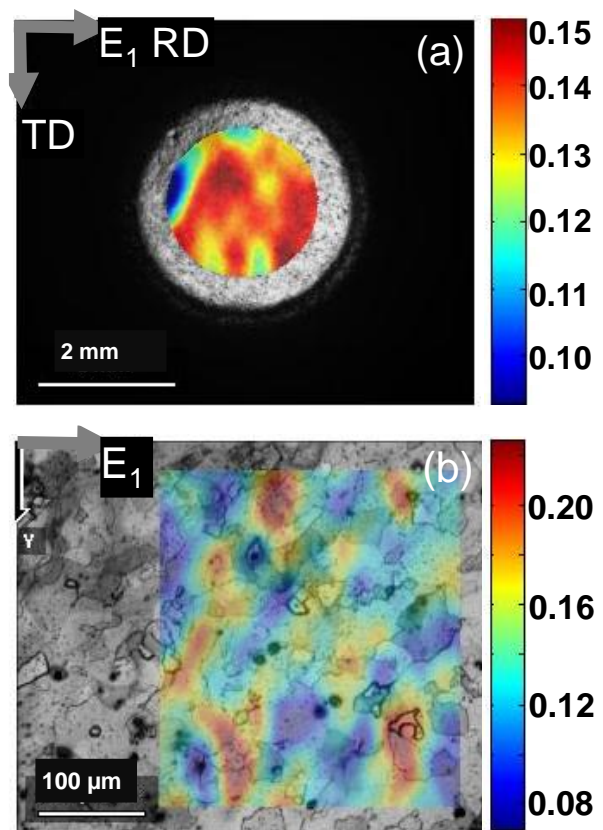


Figure 5. Major strain (ε_1) maps at macro-scale (a) and micro-scale (b) for samples tested under uniaxial tension. Images are from the RD-TD plane of the samples. Note that the strain scales are adjusted to visualize the strain localizations. In both cases, middle of the scale roughly corresponds to the average strain.

Strain distributions for samples tested under biaxial tension are mapped at the macro-scale (Fig. 6a) and at the microstructure scale (Fig. 6b). In both samples, the average major strain is $\varepsilon_1 \sim 0.06$. Assuming $\varepsilon_1 \approx \varepsilon_2 = \bar{\varepsilon}/2$ under equibiaxial tension, the equivalent strain is 0.12 and close to the one in uniaxial tension. In this case, there are localizations at both scales. Difference between the maximum and minimum strain reaches to $3x$ at the micro-scale, whereas the difference is $2x$ at the macro-scale. There is a similar trend in the deviation from the average; $1.5x$ at the micro-scale versus $1.3x$ at the macro-scale. Also, strain distribution is more

homogenous at the macro-scale, where the majority of the strain values are close to the average. This distribution may even get more homogenous at the macro-scale once the minor strains (ϵ_2) are added to the major strains.

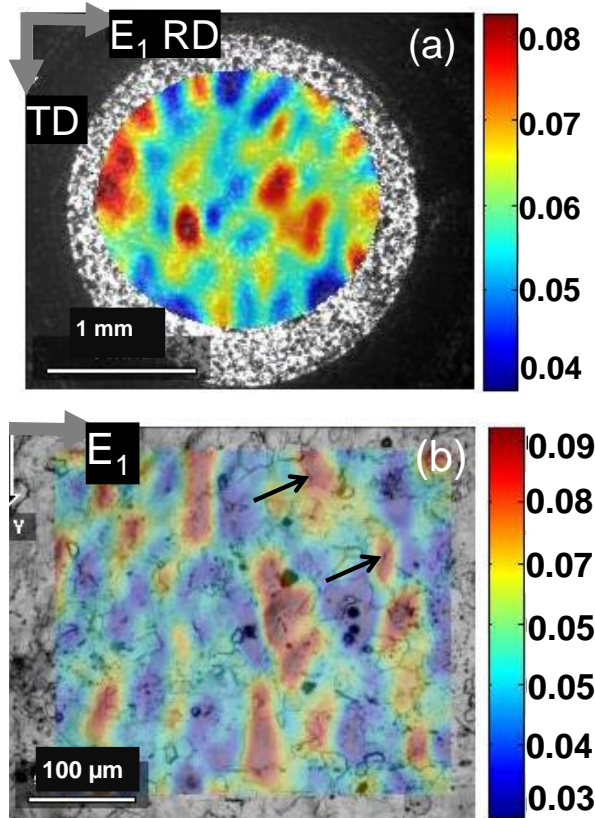


Figure 6. Major strain (ϵ_1) maps at macro-scale (a) and micro-scale (b) for samples tested under biaxial tension. Images are from the RD-TD plane of the samples. Note that the strain scales are adjusted to visualize the strain localizations. In both cases, middle of the scale roughly corresponds to the average strain.

Localizations to the grain interiors are also common under biaxial tension. Few grain boundary localizations are also observed in this case (indicated with arrows on Fig. 6b). Compared to the uniaxial results, there are also greater contrasts in the map, where maximum and minimum strain regions neighbor each other. Severity of the localizations, on the other hand, is similar under both uniaxial and biaxial tensions. Maximum strains are 3x higher than the minimum. Given that the intensity of the localizations are same under both conditions, it is possible to suggest that the localizations are independent of strain path, but they are rather a result of variation in the local microstructure and texture. Under both strain paths, some grains seem to accumulate more strain compared to the others.

EBSD orientation map of the sample deformed under biaxial tension also provides evidence for strain accumulation within the grains (Fig. 7). Almost all grains with various orientations show subgrains and

grain fragmentation. These structures indicate a high dislocation activity within the grains, which was made possible only by plastic strain. The rare initial orientations that are close to $\{100\}$ fragment, as they appear in red hues on Figure 7. Indeed, these grains allow strain in the thickness direction. Previous studies on ferritic stainless steels also showed a similar strain localization to the $\{100\}\langle 110\rangle$ grains, resulting ridging of the sheet [8]. Also during deep-drawing of the steels with initial γ fiber texture, α fiber components may reoccur [13]. Grains with $\{111\}\langle 112\rangle$ and $\{111\}\langle 110\rangle$ orientations also accumulate strain and fragment, forming $\{223\}\langle 110\rangle$ and $\{112\}\langle 110\rangle$ type grains (indicated with arrows on Fig. 7). This texture is commonly observed in the deep-drawn parts, which are also subjected to biaxial stress states during forming [13]. Indeed, emergence of α fiber texture may have promoted the localization of strain in the grains. Grains with initial orientations away from the initial γ fiber texture may have collected more strain to accommodate deformation in the thickness direction and bring the final texture close to the α fiber. Meanwhile, the grains with initial $\{111\}$ orientations have also deformed, preventing any deformation incompatibilities. Simultaneous deformation of grains with different orientations may have suppressed the grain boundary localizations.

As there is no direct location overlap between the EBSD and strain maps, experiments in this study do not provide direct evidence of localization to the $\{100\}\langle 110\rangle$ grains. However, these grains were indicated as soft orientations and shown to collect intergranular strains. Grains with $\{111\}\langle 110\rangle$ orientations, on the other hand, were shown to be “hard” and collected intragranular strains, leading to the micro strain bands [11]. Strain localizations can also be due to grain size, initial orientation and possible grain rotations during deformation [14], yet in this study the most likely candidate for them appears to be the orientation differences. Irrespective of the exact source and location of the strain concentrations, there is still strain localization happening in the mild, highly-textured steels. Eliminating all the α fiber components from the initial texture can be a viable solution to the localization phenomenon. As indicated in the literature, this is possible with a tighter control of the annealing parameters and steel’s composition [2].

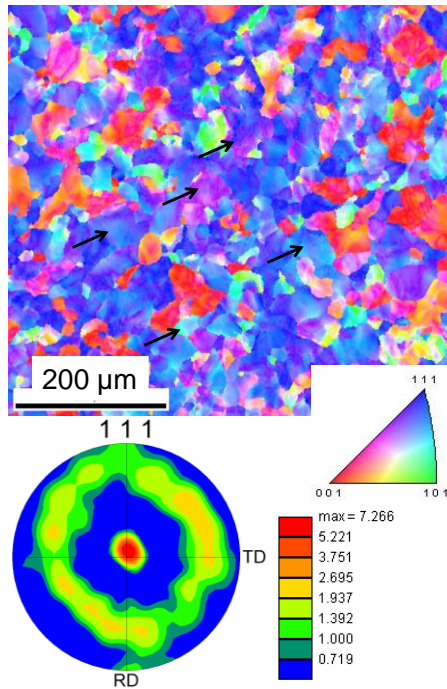


Figure 7. EBSD orientation map and (111) pole figure from the RD-TD plane of the deformed sheet under biaxial tension.

4. Conclusions

Cold-rolled sheets of DC04 grade, deep-drawing steels were characterized by their $\langle 111 \rangle // ND$ (γ fiber) texture and exceptional ductility. Same sheets were then tested under uniaxial and biaxial tension by a custom-designed, in-plane biaxial testing (cruciform) setup. The setup allowed imaging of deformation during testing, which enabled measurement and mapping of strains through DIC. The strain maps were complemented by the EBSD analysis of the microstructure before and after the deformation. This experimental framework led to the following results:

- At a fixed equivalent strain of 0.13, macro-scale (millimeter) deformation is relatively homogenous, especially under uniaxial tension. Micro-scale deformation, on the other hand, is non-uniform, where maximum strains are 3x the minimum strain. In addition, maximum and minimum strains deviate 1.5x from the average. Severity of the localizations is similar under both strain paths.
- Independent of the strain path, main strain localization regions are the grain interiors. Unlike the common grain boundary localization observed in the literature, the strain localizes into the grain interiors with specific orientations.
- Grains with orientation close to $\{100\}\langle 110 \rangle$ are the likely sources of localizations, as they accumulate more strain to evolve the initial γ fiber texture into an α fiber final texture. Meanwhile, $\{111\}\langle 110 \rangle$ type grains still deform, thus preventing any strain incompatibilities and grain boundary localizations between $\{100\}$ and $\{111\}$

grains. Therefore, cold-rolling process and the initial texture may be responsible for the uncommon localization behavior.

- While this kind of localization may not appear to be critical for macro formability in manufacturing operations, it should be of consideration during forming of miniature or thin parts, which can exhibit microstructure-sensitive deformation. Also, localization to the grains accommodating the thickness strain can create dimensional inconsistencies and undesirable surface finish. Elimination of the α fiber components from the initial texture can be a possible solution.

Acknowledgement

This work was supported by The Scientific and Technological Research Council of Turkey (TUBITAK) 3501 Career Development Program (CAREER) through a research Grant No. 115M642. Baran Güler and Berk Aytuna of METU are also acknowledged for their help in materials characterization and testing.

Author's Contributions

Mert Efe: Drafted and wrote the manuscript, performed the experiments and result analysis.

Ethics

There are no ethical issues after the publication of this manuscript.

References

1. ThyssenKrupp Steel Europe, Deep-drawing steels DD, DC and DX Product Information. <https://www.thyssenkrupp-steel.com/en/products/sheet-coated-products/mild-steel/mild-steel.html> (accessed at 15.10.2018).
2. Banerjee, K. Physical metallurgy and drawability of extra deep drawing and interstitial free steels. In: Krzysztof S (ed) Recrystallization, IntechOpen, 2012, pp 137-178.
3. Hosford, WF, Caddell, RM. Metal Forming: Mechanics and Metallurgy; Prentice-Hall Inc.: New Jersey, USA, 1993.
4. Dillamore, IL, Roberts, JG, Bush, AC. 1979. Occurrence of shear bands in heavily rolled cubic metals. *Metal Science*; 13: 73-77.
5. Raabe, D, Sachtleber, M, Weiland, H, Scheele, G, Zhao, Z. 2003. Grain-scale micromechanics of polycrystal surfaces during plastic straining. *Acta Materialia*; 51: 1539-1560.
6. Efstathiou, C, Sehitoglu, H, Lambros, J. 2010. Multiscale strain measurements of plastically deforming polycrystalline titanium: Role of deformation heterogeneities. *International Journal of Plasticity*; 26: 93-106.
7. Bieler, TR, Eisenlohr, P, Roters, F, Kumar, D, Mason, DE, Crimp, MA, Raabe, D. 2009. The role of heterogeneous deformation on damage nucleation at grain boundaries in single phase metals. *International Journal of Plasticity*; 25: 1655-1683.
8. Shin, HJ, An, JK, Park, SH, Lee, DN. 2013. The effect of texture on ridging of ferritic stainless steel. *Acta Materialia*; 51: 4693-4706.
9. Jafari, M, Ziaei-Rad, S, Saeidi, N, Jamshidian, M. 2016. Micromechanical analysis of martensite distribution on strain



localization in dual phase steels by scanning electron microscopy and crystal plasticity simulation. *Materials Science and Engineering A*; 670: 57-67.

10. Abuzaid, WZ, Sangid, MD, Carroll, JD, Sehitoglu, H, Lambros, J. 2012. Slip transfer and plastic strain accumulation across grain boundaries in Hastelloy X. *Journal of Mechanics and Physics of Solids*; 60: 1201-1220.
11. Hutchinson, B. 1999. Deformation microstructures and textures in steels. *Philosophical Transactions of the Royal Society A*; 357: 1471-1485.
12. Seymen, Y, Güler, B, Efe, M. 2016. Large strain and small-scale biaxial testing of sheet metals. *Experimental Mechanics*; 56: 1519-1530.
13. Yang, HS, Seong, BS, Han, SH, Choi, SH. 2011. Texture evolution of monolithic-phase and dual-phase steel sheets during a deep-drawing process. *Metals and Materials International*; 17: 403-412.
14. Antolovich, SD, Armstrong, RW. 2014. Plastic strain localization in metals: origins and consequences. *Progress in Materials Science*; 59: 1-160.